"This accepted author manuscript is copyrighted and published by Elsevier. It is posted here by agreement between Elsevier and MTA. The definitive version of the text was subsequently published in [GEODERMA (ISSN: 0016-7061) 235-236: 260-270 (2014), DOI 10.1016/j.geoderma.2014.07.017]. Available under license CC-BY-NC-ND."

Effect of metal oxide on surface area and pore size of water-dispersible colloids from three German silt loam topsoils.

Canlan Jiang[a,1], Jean-Marie Séquaris[a,*], András Wacha[b], Attila Bóta[b], Harry Vereecken[a], Erwin Klumpp[a]

[a] *Agrosphere, IBG 3, Forschungszentrum Jülich GmbH, D-52425 Jülich, Germany*
[b] *Department of Biological Nanochemistry, Institute of Molecular Pharmacology, Research Centre for Natural Sciences, Hungarian Academy of Sciences (IMP RCNS HAS), Pusztaszeri út 59-67, H-1025 Budapest, Hungary*[1]

*Corresponding author: Tel. +492461616635; fax: +492461612518

E-mail address: j.m.sequaris@fz-juelich.de (J.-M. Séquaris)

Abstract: The surface area and pore structure of easily dispersed soil particles < 2 μm in size (water-dispersible colloids, WDCs) are important for carbon sequestration and transport in soil. Two processes are essential for the terrestrial carbon cycling. In this work, we determine the effects of dithionite-citrate-bicarbonate (DCB) extractable metal oxides, and oxalate extractable metal oxides on the specific surface area (SSA) and pore structure of WDCs from silt loam topsoils of three TERENO test sites with a similar clay content (20%) in Germany

Abbreviations: BJH, Barret-Joyner-Halenda; CB, citrate-carbonate; DCB, dithionite-citrate-bicarbonate; DLS, dynamic light scattering; D_m, mass fractal dimensions; DOC, dissolved organic carbon; D_s, surface fractal dimension, d_p, particle diameter; d_z, z-average particle diameter; k, pore fractal dimension; M_{CB}, citrate-bicarbonate extractable metal; M_{DCB}, dithionite-citrate-bicarbonate extractable metal; $M_{oxalate}$, oxalate-extractable metal; ME, microelectrophoretic; V_p, total pore volumes; q, scattering vector; Roll, Rollesbroich; R_p, pore radii; SAXS, small-angle X-ray scattering; Selh, Selhausen; SSA, specific surface area; TOC, total organic carbon; WDC, water-dispersible colloid; Wuest, Wuestebach; ζ, zeta potential; $_{70}$, before OC removal; $_{400}$, after OC removal.

[1] present address:The College of Resources and Environmental Sciences, Nanjing Agricultural University, Nanjing, 210095, People's Republic of China

(arable (Selhausen), grassland (Rollesbroich) and forest (Wuestebach) soils). The N_2 gas-adsorption (−196°C), small-angle X-ray scattering (SAXS), dynamic light scattering (DLS) and microelectrophoretic (ME) methods were used and compared. Results show that 1) the SSA of the WDCs from Selhausen, Rollesbroich, and Wuestebach decreased more after DCB treatment (27%, 35%, and 44%) than after oxalate treatment (5%, 14%, and 22%). DCB removed metal oxide nanoparticles from WDCs were found to have diameters (d_p) ranging from 4 nm to 8 nm and the surface loading ratios on the surface of aluminosilicate residues in WDCs were estimated to be 11% to 22% for three soils where the highest value was found in the acidic forest soil. 2) Pore sizes in the mesopore range (2 nm to 50 nm) were analyzed in the WDC fractions. The results were discussed in terms of accessible open pores for the pristine WDCs and WDC samples from which metal oxide nanoparticles and organic carbon (OC) had been removed. The lower average pore radius (R_p) measured by the N_2 gas-adsorption method based on the total volume (V_t) to SSA ratio variations in WDCs without metal oxides compared to WDC with metal oxides indicated a contraction of the porous structure of WDCs due to the presence of metal oxide nanoparticles. The pore size distribution (PSD) analysis showed a sensitive contribution of metal oxide nanoparticles in the low range of pore sizes (< 25 nm) of WDCs. In SAXS measurements, higher surface fractal dimensions (D_s) were observed in WDCs before the metal oxides removal, which supports a roughness increase of the interfaces in the presence of nanoparticles. The colloidal characterization of WDCs by the DLS and ME methods shows, at a μm scale, the role of positively charged metal oxide nanoparticles in forming WDCs with a more compact structure by decreasing the particle size (d_z) and the negative zeta potential (ζ). 3) The comparison of R_p, k, d_z and d_p results between different soils also indicates the dependence on the clay mineralogy of WDCs so that the heterocoagulation between kaolinite and illite (clay minerals of different aspect ratios) increases the size of soil mesopores (Rollesbroich). In conclusion, the results of this study clearly show that the combination of the N_2 gas-adsorption, SAXS, DLS and ME methods allows the characterization of soil porosity in the nanometer range where metal oxide nanoparticles contribute to a more compact structure of WDC.

Key words: Metal oxide; Water dispersible colloid; Particle size; Surface area; Mesopore; Small-angle X-ray scattering; N_2 gas-adsorption; Dynamic light scattering; Microelectrophoretic method.

1. Introduction

Soil structures have an important influence on environmental processes such as water filtration and carbon sequestration. The large specific surface area (SSA) of the soil clay fraction traps and stabilizes organic carbon (OC) through electrostatic and chemical complexations (Mikutta et al. 2007). The inclusion of the soil clay fraction in the narrow porous structure of soil hinders the accessibility of OC to microbial degradation (Sollins et al. 1996; Baldock and Skjemstad 2000; Six et al. 2002). Water dispersible colloids (WDCs) that can be easily dispersed in contact with soil water are soil particles < 2 μm from soil clay fractions. They mainly include aluminosilicate and metal oxide particles, which can be released from soil aggregate structures. The dispersions of the soil clay content into a WDC form promotes the accessibility of uncomplexed organic matter and leads to its further transport as dissolved organic matter (DOM) (McCarthy and Zachara, 1989; Kretzschmar, et al., 1999). By strongly associating with the clay surfaces of WDC, transport of OM into deeper soil layers is also possible (Séquaris et al., 2010). Mechanical and chemical processes in soil are key factors which affect the stability of soil aggregates and thus the release and stability of mobile WDCs such as a combination of hydrodynamic parameters (intensive rain, splash erosion, infiltration water rate) and chemical dispersion conditions (the presence of organic matter, increasing pH, decreasing ionic strength and increasing sodium adsorption ratio (SAR)) (Jarvis et al., 1999; Kjaergaard et al., 2004a, b). It has been shown that shaking soil aggregates in low-ionic strength water simulates erosive dispersion (Séquaris et al., 2010). WDC release has been modeled by formulating a two-step mechanism (Ryan & Gschwend, 1994; Ryan & Elimelech, 1996). A rapid detachment step of WDC is shown by modeling the net-interaction energy potential between colloids and mineral grains. It is followed by a diffusion-controlled transport step of the mobilized WDC through immobile water layers at the soil aggregate surfaces in the low mechanical energy range of batch experiments (Ryan & Gschwend, 1994； Jiang et al., 2014).

The heterogeneous WDC structure contributes to the sequestration of organic matter. The organic matter is stabilized by physical inclusion and chemical reaction with metal oxide surfaces (Kaiser and Guggenberger, 2000; Wagai and Mayer, 2007; Kiem and Kögel-Knabner 2002; Kaiser and Guggenberger 2003; Eusterhues et al. 2005). Various forms of iron oxides can be found in soils (Cornell and Schwertmann, 2003). Iron oxides in crystalline form such as goethite and in less-crystalline forms such as hydrous oxide ferrihydrite are the most abundant (Childs, 1992; Gaboriaud and Ehrhardt, 2003; Roden and Zachara, 1996). In the

case of aluminium oxide, less-crystalline forms such as hydrous oxide gibbsite are the most common (Gilkes et al., 2006; Rosenqvist et al., 2003). These metal oxides can be selectively extracted by different dissolution methods. Dithionite–citrate–bicarbonate (DCB) treatment (Turchenek and Oades, 1979, Cornell and Schwertmann, 1996, Kiem and Kögel-Knabner, 2002; Mehra and Jackson, 1960) mainly extracts Fe oxyhydroxides, which can be used to calculate the total iron oxide (M_{DCB}) via reduction and parts of the dissolve oxides for Al and Si. Ammonium oxalate treatment (pH 3) (Kiem and Kögel-Knabner, 2002; Schwertmann, 1964) is generally used for the selective dissolution of Fe, Al, and Si ($M_{oxalate}$) from poorly crystalline aluminosilicates, ferrihydrite and Al- and Fe-humus complexes, but the Al, Fe, Si from gibbsite, goethite, hematite and layer silicates are not included (Mikkuta et al., 2005). Despite the relatively low mass contribution of metal oxides to German soil, these nanometer-sized mineral particles have significant effects on the total surface of soil aggregates because of their inherently large surface area. (Eusterhues et al., 2005; Kaiser and Guggenberger, 2003; Pronk et al., 2011). These particles are located as free clusters or cover the surface of much larger particles (Desphande et al. 1968; Hendershot and Lavkulich 1983). They contribute to the porous structure of WDC by their interactions with large plate-like particles of clay minerals. Thus, small organic molecules, such as organic acids, should be able to enter micropore space (< 2 nm), where they would be protected from microorganisms and their enzymes (Eusterhues et al., 2005). A comprehensive characterization of the heterogeneous porosity of WDCs in air-dried and water-dispersed states requires different chemical and physical approaches. Pores can be defined as open pores if they communicate with the external surface and are accessible to molecules or ions from the surroundings. By contrast, closed pores are closed as individual voids in the mineral matrix which is not interconnected to the external surface (Radlinski et al., 2004). The N_2-gas adsorption method has been widely used to measure the specific surface area (SSA) and characterize the open porosity of air-dried soil particles, especially the mesoporosity (pore width between 2-50 nm) and microporosity (pore width not exceeding 2 nm) (Mayer et al., 2004; Pronk et al., 2011). The small-angle X-ray scattering (SAXS) technique (Guinier and Fournet, 1955) has been used more generally for the internal and external structural characterization of porous solid materials on a length scale of typically 1 nm to 100 nm as in the case of silica gel (Schmidt, 1991; Schmidt et al., 1991) and clay minerals (Pernyeszi and Dékány, 2003). It has been shown that SAXS technique is suitable for studying fractal dimensions, (*D)* of powders with porous or irregular surface (Höhr et al., 1988; Schmidt, 1991) where *D* values are provided from a power law of the measured scattered intensity *I(q)* as a function of the scattering angle

2θ. *D* values have thus expressed the compactness of allophane aggregate clusters in andosols (Chevallier et al., 2010) and the surface roughness of soil grains (Borkovec et al., 1993). Broadly speaking, higher *D* values point to higher surface roughness, higher aggregation mechanism and higher cluster compactness (Marliere et al., 2001).

The effect of metal oxides on soil SSA and pores can be determined through N_2 gas-adsorption method while investigations using the SAXS method are not aware to our knowledge. Kaiser & Guggenberger found that the SSA of soils is highly correlated with the amount of Fe oxyhydroxides (Kaiser and Guggenberger, 2003). Eusterhues et al. (Eusterhues et al., 2005) studied two German acid forest soils and found only a few micropores remaining in samples after the dissolution of iron oxides. The soluble minerals in the DCB extraction method were identified as the main microporous phases in soil. Filimonova et al. (Filimonova et al., 2006) demonstrated that the removal of iron oxides by DCB treatment decreases the SSA by up to 50%. In their study, the micropores completely vanished in two German luvisol and gleysol soils.

In the present study, both gas adsorption and SAXS were applied to investigate the effect of metal oxide particles in the SSA and porous structure of the mineral matrix in WDC samples in the freeze-dried state. The variations of colloidal properties of WDCs were detected in the water-dispersed state of WDC samples by dynamic light scattering (DLS) and microelectrophoretic (ME) methods. Soil samples were obtained from the TERENO project, whose observatories span Germany and supply data regarding the impact of long-term climate change on ecosystems, land use, and infrastructure at the regional level (www.TERENO.net) (Zacharias et al., 2011). This study is part of the SoilCan project (Puetz et al., 2009) of TERENO and mainly focuses on the stability of soil aggregates. (Séquaris et al., 2013; Jiang et al., 2014). Three German silt loam topsoils were systematically analyzed after applying the DCB and oxalate extraction methods. The three soils were luvisol, cambisol, and gleysol, all of which are widespread and important for agriculture all over the world (Driessen et al., 2001). With N_2 gas-adsorption, SSA variations in WDC fractions and bulk soils were examined. In the case of WDC fractions, total pore volumes (V_p) were also measured to further calculate the distribution of pores and the average pore radii (R_p). Particular attention was paid to estimating the size extent of the coverage of metal oxide nanoparticles in the mesopore size range of the WDC mineral matrix. Information obtained by the SAXS method about the surface fractal dimensions from power law scattering intensity was recorded. The diameter and zeta potential of colloidal WDCs were further investigated by the DLS and ME

methods, respectively. The results of the colloidal characterization of the samples in the micrometer range were related and compared to the N_2 gas-adsorption and SAXS results. This study aims to reconcile results using very different measurements and to provide information on WDC structure parameters affected by metal oxides.

2. Materials and methods

2.1. Soil samples

Topsoil samples (0 cm to10 cm) were collected in July 2010 from three test sites in Germany, Selhausen (Selh) (50°52′08″N; 6°26′59″E; arable luvisol), Rollesbroich (Roll) (50°37′18″N; 6°18′15″E; grassland cambisol) and Wuestebach (Wuest) (50°37′18″N; 6°18′15″E; forest gleysol). The topsoil samples were air- dried. Visible stones and large pieces of plant materials were removed by hand. The soil samples were ground to pass through two sieves (mesh widths 5 and 2 mm). The < 2 mm fraction was defined as bulk soil.

2.2. Analytical characterization of topsoil samples.

Total organic carbon (TOC) was determined with a LECO RC-612 carbon analyzer after correcting the total carbon from the inorganic carbon content. Total nitrogen (TN) contents were analyzed with a C/N analyzer (Vario EL cube; Elementar, Hanau, Germany). Total metal contents were determined with an inductively coupled plasma–optical emission spectroscopy (ICP–OES) Thermo Elemental (TJA) Iris Intrepid spectrometer. The pH was measured with an Expandable Ion Analyzer EA 940 from Orion Research. The mineralogy of the clay fraction (Table 1) was determined by standard XRD with Mg-glycerol- and K-glycerol-saturated samples. XRD analysis was performed using a Philips diffractometer (Model PW 1130/90, Almelo, The Netherlands) with Co-Kα radiation (1600 watts, Ni filter) at a scanning speed of 2° per minute.

2.3. Soil WDC fractionation

In order to obtain the WDC fraction in batch experiments with minimum artificial impacts on soil structure, a soft soil particle-size fractionation method (Séquaris and Lewandowski, 2003) including shaking and sedimentation processes was chosen. Indeed, an estimation of the kinetic energy to disperse WDC was made (Jiang et al., 2014). This is relatively low in comparison with the total energy applied in end-over-end shaking and

ultrasonic methods. According to the method, a 1000 mL Duran bottle (Schott, Germany) containing 100 g of air-dried soil and 200 mL of Millipore deionized water was shaken horizontally using a thermostated incubator at a rotational speed of 170 rpm for 6 h at 23°C. The mixed suspension was allowed to settle after the addition of 600 mL of Millipore deionized water. After a sedimentation time of 12 h at 23°C, a separate aqueous phase containing the nonsettling colloidal particle fraction (< 2 μm) was obtained. This easily dispersed colloidal soil content in the aqueous phase was designated WDCs. A solid size fraction ranging from 0.05 μm to 2 μm was obtained after high-speed centrifugation (10,000 *g*; 90 min) of the colloidal dispersion without any filtration. The remaining upper aqueous phase was designated the electrolyte phase. The organic carbon content of this phase (<0.6% of TOC) was not considered in the present study. WDCs and bulk soil samples were freeze-dried before analysis of the TOC, TN, and total metal contents. The N_2 gas- adsorption and SAXS methods were applied before and after thermal oxidation of the freeze-dried samples.

2.4. Determination of dithionite-extractable Fe, Al and Si (DCB method)

Dithionite-extractable Fe (Fe_{DCB}), Al (Al_{DCB}) and Si (Si_{DCB}) were determined in the three replicates through DCB extraction(Kiem et al., 2002). DCB stock solution was prepared by mixing 600 mL of sodium citrate (0.3 M), 0.2 L of sodium hydrogenocarbonate (1 M), and 15 g of sodium dithionite. The soil samples (200 mg) were dispersed in 40 mL of DCB stock solution in a centrifugation tube. After shaking on a horizontal shaker for 16 h at room temperature, the soil dispersion was centrifuged at 7741 *g* for 30 minutes and the supernatant was retained. The centrifugate was dispersed again in 32 mL of magnesium sulfate (0.05 M) to exchange the sorbed metals from DCB extraction and then centrifuged for the second time. The two supernatant phases were combined and the Fe_{DCB}, Al_{DCB} and Si_{DCB} contents were analyzed with an ICP-OES Thermo Elemental (TJA) Iris Intrepid spectrometer. The soil samples treated without the dithionite reagent (CB treatment, M_{CB}) were used as reference to distinguish possible complexation and exchange effects of free metals by citrate/bicarbonate and magnesium, respectively from the metal oxide dissolution effects due to dithionite (Barberis et al., 1991). Fe (Fe_{CB}), Al (Al_{CB}), and Si (Si_{CB}) were assigned to soluble forms of metal complexes. The treated soil samples were collected and freeze-dried. N_2 gas- adsorption and SAXS were applied after thermal oxidation of the freeze-dried samples.

2.5. Determination of oxalate-extractable Fe, Al, and Si

The soil samples were extracted in triplicate with ammonium oxalate to measure the concentrations of $Fe_{oxalate}$, $Al_{oxalate}$ and $Si_{oxalate}$ (Kleber et al., 2005; Masiello et al., 2004; Mikutta et al., 2005). A 0.2 M oxalate solution was prepared with 0.113 M ammonium oxalate and 0.087 M oxalic acid (Kiem and Kögel-Knabner, 2002). A centrifugation tube containing 200 mg of the soil samples (bulk soil sample and WDC) and 40 mL of an acidic oxalate solution (0.2 M, pH around 3) was shaken on a horizontal shaker for 2 hours in the dark. After shaking, the soil dispersion was centrifuged (7741 g and 30 minutes). The supernatant containing $Fe_{oxalate}$, $Al_{oxalate}$ and $Si_{oxalate}$ was analyzed by an ICP-OES Thermo Elemental (TJA) Iris Intrepid spectrometer. Average values were obtained from the three replicate measurements. The soil samples were treated without the oxalate reagent (Millipore water, blank) and were used as a reference to distinguish a possible water leaching effect from the dissolution effect due to oxalate. The contents of Fe (Fe_{blank}), Al (Al_{blank}), and Si (Si_{blank}) were analyzed and the treated soil samples were collected and freeze- dried. N_2 gas-adsorption was applied after thermal oxidation of the freeze-dried samples.

2.6. Thermal oxidation

OM was removed from the freeze-dried bulk soil and WDC fractions by thermal oxidation (Mayer, 1994b; Mayer et al., 2004; McCarthy et al., 2008; Séquaris et al., 2010; Sollins et al., 2007) at 400°C for 16 h. This treatment can remove 95% of the TOC originally present in the soil sample (Séquaris et al., 2013). The samples after OC removal were labeled as CB400, DCB400, blank400, and oxalate400. The samples before OC removal were labeled as CB70, DCB70, blank70, and oxalate70 (see also 2.7 N_2 gas-adsorption).

2.7. N_2 gas-adsorption experiment

SSA ($m^2\ g^{-1}$) was analyzed by N_2 adsorption at −196°C with an AUTOSORB-1 (Quantachrome) apparatus. SSA was calculated according to the multilayer adsorption isotherm derived by Brunauer, Emmet and Teller, also known as the BET isotherm (Lowell et al., 2006) in a relative pressure range P/P_0 <0.3. Three replicate measurements were performed. The soil samples were degassed for 16 h at 70°C using N_2 as the carrier gas before determining SSA_{CB70}. This procedure removed the water content without destroying the OM. The OM of the soil samples was removed by thermal oxidation to measure the SSA_{CB400},

SSA_{DCB400}, $SSA_{blank400}$ and $SSA_{oxalate400}$ of the mineral phase. The soil samples were degassed for 2 h at 200°C using N_2 as the carrier gas before SSA determination. During the thermal oxidation process, possible mineral surface modifications of metal oxide content were brought about (Kaiser and Guggenberger, 2003). Indeed, phase changes in goethite and ferrihydrite to hematite were generally observed in the temperature range from 50°C to 400°C under Si-free conditions (Campbell et al., 2002). This results in an SSA increase of 50% for goethite and an SSA decrease of 80% for ferrihydrite (Clausen and Fabricius, 2000). Low-temperature chemical oxidation processes of OM were thus proposed (Kaiser and Guggenberger, 2003; Kiem and Kögel-Knabner, 2002; Kahle et al., 2003; Wagai et al., 2009) for the removal of OM. Results of low-temperature chemical oxidation and thermal oxidation on mineral SSA for similar soils have been discussed (Wagai et al., 2009; Sequaris et al., 2010). It was found that the lower efficiency of low-temperature chemical oxidation for total OM removal mainly limits the comparison of SSA (Wagai et al., 2009).

In the same way, we have removed the OM from WDC samples by using sodium peroxodisulfate ($Na_2S_2O_8$) according to the method of Kiem and Kögel-Knaber (Kiem and Kögel-Knabner, 2002). The $SSA_{chemical}$ results were compared to SSA_{400}. Slightly higher values were measured for $SSA_{chemical}$ (m^2g^{-1}): 92.9, 77.9 and 93.9 in comparison to SSA_{400} (m^2g^{-1}): 84.1, 74.7 and 83.6 for Selhausen, Rollesbroich and Wuestebach WDC samples, respectively. Corresponding $SSA_{chemical}/SSA_{400}$ ratios of 1.1, 1.04 and 1.1 were calculated for Selhausen, Rollesbroich and Wuestebach respectively which indicate some maximal SSA variations of about 10% between the both methods. Furthermore, the detection of possible alterations of the mineral surface due to the muffling technique in the temperature range from 70°C to 400°C was investigated in the case of Selhausen soils. Comparative SSA measurements were made of six bulk soil samples (Table 2) taken at two sampling points C1 and C16 (Borneman et al., 2011) from depths of 0-30 cm, 30-60 cm, and 60-90 cm. Soil samples with the lowest TOC contents (TOC < 13 g kg^{-1}) were thus chosen to minimize the potential interference of OC contents on the SSA measurement of the mineral surface. After dry heating at 70°C (SSA_{70}) and thermal oxidation at 400°C (SSA_{400}), an average SSA_{70}/SSA_{400} value of 0.97 ± 0.10 was calculated for the six soil samples. In the case of the subsoil samples with the lowest OC contents (TOC < 5 g kg^{-1}), an average SSA_{70}/ SSA_{400} value of 1.07 ± 0.03 was found (table 2). It can be thus concluded to that thermal oxidation at 400°C led to a surface alteration with a decrease of SSA by less than 10%. Thus the reported SSA_{400} values being considered to be the SSA value of the soil mineral surface are reasonable.

SAXS data have also shown that the arrangement of aluminosilicate particles forming mesopores in soil and sediment samples remains largely unaffected after the removal of organic matter (OM) by muffling at 375 °C (Mayer et al., 2004). It is to be noted that a rather high Si content in natural ferrihydrite may also hinder a hematite transformation under temperature conditions comparable to those used in laboratory syntheses (Campbell et al., 2002).

The total pore volume (V_p) of the soil samples was determined at a P/P_0 of 0.995. The volume - to - surface area ratio of the pore was used to scale the average pore radius (R_p) variations. According to IUPAC (1985), V_p */SSA* is the radius of parallel -sided slit shaped pores. In nonintersecting cylindrical capillaries, R_p is calculated as 2 V_p */SSA* (Lowell et al., 2006). The pore size distributions (PSDs) were obtained by the Barret–Joyner–Halenda (BJH) method from the adsorption branch of the N_2 isotherm, which was hardly affected by the tensile strength effect of N_2 in comparison to the desorption branch (Groen et al., 2003). The modified Kelvin equation based on a cylindrical pore model serves as the basis for the BJH method (Lowell et al., 2006).

The Dubinin-Radushkevitsch (DR) equation (Lowell et al., 2006) was used to calculate the micropore volume ($V_{\mu pore}$) in WDC (pore widths not exceeding 2 nm) in a relative pressure range $P/P_0 < 0.0025$.

2.8. Characterization of metal oxide effects in soil samples using N_2 gas- adsorption.

Contribution of metal oxide content to total mineral SSA

The differences between SSA_{CB400} and SSA_{DCB400} were used to estimate the contribution of DCB extracted metal oxide content to the total mineral SSA_{CB400} of WDCs and bulk soil samples:

$$SSA_{\text{total metal oxide}}contribution(\%) = \frac{(SSA_{CB400} - SSA_{DCB400})}{SSA_{CB400}} \quad (1)$$

The differences between $SSA_{blank400}$ and $SSA_{oxalate400}$ were used to estimate the contribution of oxalate extractable metal oxide content to the total mineral $SSA_{blank400}$ of WDCs and bulk soil samples:

$$SSA_{\text{non-crystalline metal oxide}}contribution(\%) = \frac{(SSA_{blank400} - SSA_{oxalate400})}{SSA_{blank400}} \quad (2)$$

Estimation of extracted metal oxide SSA ($SSA_{metal\ oxide}$) from WDC

The $SSA_{metal\ oxide}$ of the WDCs was estimated by considering a simple additive law for the SSA contributions of metal oxide particles and WDC residues after dithionite dissolution (SSA_{DCB400}) to the mineral surface of WDC (SSA_{CB400}) :

$$SSA_{\text{metal oxides}} = \frac{(SSA_{CB400} - (1-w)SSA_{DCB400})}{w} \quad (3)$$

where SSA_{DCB400} is assigned to the SSA of the aluminosilicate content in WDC and w (g g^{-1}, Table 3) is the mass (g) of released metal oxide per g of WDC (weight fraction).

Surface loading ratio (θ) estimation of metal oxide particles in WDC

For particles with a spherical shape and radius r, the sum of the projected circular surface area from the total content of N spherical nanoparticles (considered as non-porous spheres) of per g WDC was calculated as $N\pi r^2 = SSA_{\ metal\ oxide} * w / 4$ where $SSA_{\ metal\ oxide}$ is the spherical surface area (surface = $4\pi r^2$). Thus, the surface loading ratio (θ) per g of WDC was calculated as

$$\theta = \frac{SSA_{metal oxide} * w}{4SSA_{DCB400}} \quad (4)$$

Calculation of metal oxide particle diameter (d_p)

The SSA per particle mass ($m^2\ g^{-1}$) was calculated as

$$SSA_{\text{metal oxides}} = \frac{N4\pi r^2}{N\frac{4}{3}\pi r^3\rho} = \frac{3}{r\rho} \quad (5)$$

where r is the particle radius and ρ is the particle density (g cm^{-3}). The average mean diameter (d_p) of the metal oxide particles (nm) was calculated as

$$d_p = \frac{6000}{SSA_{\text{metal oxide}}\rho} \quad (6)$$

2.9. SAXS measurement

The SAXS measurements were performed to compare the effect of metal oxides on the aggregate compactness and the surface roughness of WDC samples from the fractal nature of the scattering materials. Cu Kα X-rays were provided by a GeniX3D Cu ULD X-ray beam delivery system (Xenocs, Sassenage, France), consisting of a microfocus X-ray tube operated at 30W and a parabolic multilayer mirror, which parallelizes and monochromatizes the beam. Collimation of the X-ray beam was done by three Pt-Ir pin-holes, 0.3, 0.3 and 0.5 mm diameter. Samples were measured in vacuum between two layers of foils (Tixo, Cellux). The scattering of the foils was negligible compared to that of the samples. Scattered X-rays were detected by a Pilatus-300k CMOS hybrid pixel detector (Dectris, Baden, Switzerland). Resulting X-ray scattering patterns were corrected for background scattering, geometrical distortions, and sample self-absorption. They were calibrated into absolute intensity units of 1/sterad using a pre-calibrated glassy carbon sample. All of the data reduction was done by the control software of the instrument. In order to cover a wider scattering vector $q = 4\ \pi\ \sin\theta/\lambda$ where λ is the X-ray wavelength, experiments were repeated with short (454 mm) and long (1216 mm) sample-to-detector distances. The one-dimensional scattered intensity (I) curves were scaled together and plotted as a function of the scattering vector q between 0.075 nm^{-1} and 6 nm^{-1}.

The logarithmic form of the power-law scattering relation gives the exponent k, whose magnitude has been discussed in terms of fractal dimension in the case of porous systems (Bale and Schmidt, 1984; Borkovec et al., 1993; Schmidt, 1991). The power-law scattering of SAXS results over a large range of q, has been considered in the following equation:

$$I(q) = \frac{p}{q^k} \tag{7}$$

Power-law scattering exponents $k \leq 3$ are typical of mass fractals that are often aggregates of sub-units. For objects whose surface is fractal, $3 < k < 4$ exponents are related to the surface fractal dimension D_s by

$$k = -(6 - D_s) \tag{8}$$

which generally characterize powders with porous or irregular surface (Höhr et al., 1988; Schmidt, 1991).

2.10. Dynamic light scattering (DLS) and microelectrophoretic (ME) measurements

The colloidal properties of WDCs were investigated by DLS and ME methods. DLS measurements were performed using a Malvern Nano-ZS apparatus. The measurements were made at the scattering angle of 173° for colloidal soil materials at 20 °C. The monomodal cumulant method of the Nano-ZS apparatus software was used to analyze the correlation function. The averaged translational diffusion constant obtained was used to calculate an equivalent spherical hydrodynamic diameter (*z*-average diameter, d_z) for the particles. The freeze-dried WDC suspension concentration (0.4 g L^{-1}) was vigorously shaken for 12 h after ultrasonication for 4 min, and the dispersion was sonicated for another 10 min before the measurements were made. The samples were transferred to a disposable polystyrene cuvette during the measurement. For the electrokinetic investigation, a Malvern Nano-ZS apparatus was used to measure the ζ-potential (Smoluchowski equation) from the microelectrophoretic mobility (u) at 20°C. The suspension concentration was 0.4 g L^{-1}. Our schematic diagram of the soil sample preparation is shown in Fig. 1.

3. Results and discussion

3.1 Soil sample physicochemical characteristics

The mean grain size distribution, pH, TOC, TN and total metal (Fe, Al, Si) contents in the bulk soil samples are listed in Table 1. XRD analysis revealed that all the three silt loam topsoils had 20% clay content, with illite being the most abundant clay mineral. The soil acidity, TOC content, and TN content increased along the series Selhausen < Rollesbroich < Wuestebach. The contents of Fe and Al were also higher in Wuestebach soil than in the Selhausen and Rollesbroich soils. The highest mass of the released WDC fraction in Selhausen soil sample (Table 3) has recently been discussed (Jiang et al., 2014).

3.2. Metal oxide content and surface properties of WDCs and bulk soil samples

*3.2.1. Distribution of metal oxides in WDCs and bulk soil*s

The DCB chemical extraction method was used to characterize the metal oxide content of WDC and the bulk soil samples (Cornell and Schwertmann, 2003). It is generally assumed that Fe extracts obtained by the DCB method (Fe_{DCB}) include both crystalline and less-crystalline forms of Fe oxides. Al_{DCB} represents Al substituted in Fe oxides and from the

partial dissolution of poorly ordered Al-(oxy)hydroxides (Mikutta et al., 2005). The comparison of contents extracted by the CB and DCB method confirmed higher distributions of Al_{CB} and Si_{CB} which are not related to the reductive dissolution of iron oxides. The subtraction of the corresponding M_{CB} extracted contents (readily soluble forms of metal complexes) from M_{DCB} (Material and methods, Table 4) thus yielded M extracts closely associated with the both crystalline and less- crystalline forms of metal oxides. The mass distributions of Fe, Al, and Si in the M_{DCB-CB} of all WDCs and bulk soils ranged from 88%to 90%, 7% to 11% and 0.5% to 2.9%, respectively. The corresponding molar distributions of Fe, Al, and Si in M_{DCB-CB} ranged from 79% to 82%, 13% to 20% and 1% to 6%, respectively. These results confirm the significant contribution of Fe to the total metal oxide content of the WDCs and bulk soil samples. The extracted Fe_{DCB-CB} mass from the bulk soils corresponded to 44% (Selhausen), 55% (Rollesbroich), and 53% (Wuestebach) of the total Fe content (Table 1).

The $Al_{oxalate}$, $Fe_{oxalate}$ and $Si_{oxalate}$ contents determined through oxalate extraction are listed in Table 5. Negligible contents of the corresponding metals under shaking conditions in water, M_{blank}, were also reported. In comparison to DCB extraction results, lower $Al_{oxalate}$, $Fe_{oxalate}$ and $Si_{oxalate}$ contents in the WDCs and bulk soil samples were operationally related to the less-crystalline forms of metal oxides. The mass distributions of Fe, Al, and Si in the $M_{oxalate}$ of the WDCs and bulk soil samples ranged from 63% to 76%, 20% to 35% and 1% to 5%, respectively. The corresponding molar distributions of Fe, Al, and Si in $M_{oxalate}$ ranged from 45% to 59%, 32% to 52% and 1% to 8%, respectively, confirming the significant contribution of Fe in the less-crystalline form of metal oxides. The distribution of the less-crystalline form of Fe ($Fe_{oxalate}$ /Fe_{DCB}) was markedly higher (0.45 to 0.54) in Wuestebach samples (forest soil) than in other topsoils samples (0.26 to 0.38). $Fe_{oxalate}$ /Fe_{DCB} distributions of 0.27 to 0.94 have been reported for a large collection of agricultural topsoil (Hiemstra et al., 2010a) and of 0.31 to 0.74 in particle size fractions of loamy arable topsoils (Pronk et al., 2011).

3.2.2. Effect of metal oxides on SSA in WDCs and bulk soils

An interesting aspect is the determination of SSA variations, which accompany the removal of metal oxide particles from the WDCs and bulk soils (Kiem and Kögel-Knabner, 2002; Kretzschmar et al., 1993; Pronk et al., 2011; Séquaris et al., 2013). The effects of the extraction method (DCB and oxalate) on the mineral SSAs of the different soil samples are

compared in Table 6. The SSA of different samples, before and after treatments was compared after OC removal by thermal oxidation (SSA_{400}). The results before OC removal (SSA_{70}) were also shown. As shown in Table 6, SSA_{DCB400} and $SSA_{oxalate400}$ decreased after the extraction of metal oxides compared to the blank samples (SSA_{CB400} and $SSA_{blank400}$). These results confirm the significant contributions of metal oxides to mineral surface properties (Borggaard, 1982; Eusterhues et al., 2005; Pronk et al., 2011; Trolard et al., 1995). The contributions of total metal oxide contents to the total mineral SSA of the WDCs and bulk soil samples were calculated according to Eq. (1). The percentage of variation of the total SSA [(SSA_{CB400}- SSA_{DCB400}) / SSA_{CB400} and ($SSA_{blank400}$- $SSA_{oxalate400}$) /$SSA_{blank400}$] in Table 6 can be positively related to the increase in the contents of M_{DCB-CB} (Tables 4 and 5) along the series Selhausen < Rollesbroich < Wuestebach. In the Selhausen topsoil, for example, SSA contributions from the total and less-crystalline metal oxide contents were 41% and 27% in the bulk soil and 16% and 5% in the WDCs, respectively. In this topsoil, the lower SSA contributions of the oxalate extracted metal oxide contents were related to the lower oxalate extracted metal oxide distribution given by $Fe_{oxalate}$ /Fe_{DCB} of 0.29 in Table 5. The results show that the contribution of metal oxide to the total SSA in the case of WDC_S, a potential representative of the clay fraction, is lower than in the bulk soils. This result can be explained by a large distribution of metal oxides outside the free clay fraction in bulk soil samples (Blum, 2007).

As shown in Tables 6 and 3, the DCB extracted metal oxides increased the SSA of the WDCs samples along the series Selhausen (27%) < Rollesbroich (35%) < Wuestebach (44%) while the TOC content increased along the series Selhausen (21 g kg^{-1}) < Rollesbroich (67 g kg^{-1}) < Wuestebach (71 g kg^{-1}) in WDCs. These data further support the direct surface interactions. In the clay fraction, OM sequestration as organo-mineral complexes is mainly due to interactions with less-crystalline and crystalline metal oxide contents in the studied acidic soils (Mikutta et al., 2005).

3.2.3. Estimation of the SSA and particle size of the metal oxide extracted from the WDC samples

The SSA of DCB extracted metal oxides ($SSA_{metal\ oxide}$) was estimated by Eq.(3).As shown in Tabl**e** 3, SSA values for DCB extracted metal oxides ranged from 217 m^2g^{-1} to 420 m^2g^{-1}, which are typical of iron oxide nanoparticles, such as ferrihydrite (Cornell and Schwertmann, 2003). The SSA_{DCB400} values ranged from 32 m^2g^{-1} to 64 m^2g^{-1} (Table 6), which

is typical of illite (Kaiser and Guggenberger, 2003), the major aluminosilicate in the clay fraction of topsoils (Table 1). It must be remarked that freeze-dried WDC samples were characterized by the typical platelet–like structure of clay minerals (Séquaris et al., 2013). The metal oxide nanoparticles was assumed to cover on aluminosilicate surfaces in WDC and the possible coverage of was estimated by Eq. (4) with the surface loading ratio (θ). An increase in θ along the series Selhausen (11%) < Rollesbroich (16%) < Wuestebach (22%) was calculated for the maximal surface loading in the monolayer (Table 3). At lower pH, the WDCs from the acidic forest soil apparently had the largest surface loading of metal oxides. This is promoted by the precipitation of metal oxides carrying sufficient positive charge at the negatively charged clay surface (Goldberg, 1989). Based on the $SSA_{metal\ oxide}$ values, we calculated the diameter of the nanoparticles (d_p) with Eqs. (5) and (6), in which ρ for total metal oxides from three soils of approximately 3.6 g cm^{-3} (values: 3.56-3.57 gcm^{-3}) was calculated from a mass distribution of $Fe_{DCB\text{-}CB}$, $Al_{DCB\text{-}CB}$ and $Si_{DCB\text{-}CB}$ and the density of typical Fe oxide (ferrihydrite, 3.8 g cm^{-3}), typical Al oxide gibbsite (2.44 g cm^{-3}) and typical Si oxide, Silica(2.32 g cm^{-3}), respectively, in the metal oxide particle mixture. dp values in the range of 4 nm to 8 nm were estimated for the metal oxide nanoparticles (Table 3). Similar particle sizes (1 nm to 10 nm) of metal oxides were reported after DCB extraction of agricultural topsoils (Hiemstra et al., 2010a) and haplic podzol soils (Eusterhues et al., 2005).

3.3. Substructural study on the effect of metal oxides in WDCs

The major sequestration of OM in the heterogeneous microstructure of the soil clay-size fraction (Chenu and Plante, 2006) is controlled by the accessibility of the mineral porous matrix formed by metal oxides and aluminosilicate particles. SAXS and N_2 gas-adsorption methods were used to characterize the WDCs structures before and after metal oxide removal by the DCB method and to establish relationships between the two methods and to obtain complementary information on the porous structure of the WDC samples. The diameter and zeta potential of colloidal WDCs before and after DCB treatment were further investigated by dynamic light scattering (DLS) and microelectrophoretic (ME) methods, respectively. The results of the colloidal characterization in the micrometer range were related and used in the interpretation of the N_2 gas-adsorption and SAXS results.

3.3.1. Application of N_2 gas- adsorption methods for the pore size investigation of WDCs (effect of metal oxide particles and OC contents)

For WDC_{DCB400} and WDC_{CB400}, the SSA and total pore volume (V_p) of all pore radii up to 180 nm were obtained with the N_2 adsorption isotherms at a P/P_0 of 0.995 (Table 7). The volumes of the micropores ($V_{\mu pore}$) with pore radii of less than 2 nm were also reported for comparison.. In this study, they correspond to a low fraction (5% ± 2%) of V_p. Sensitive variations of SSA, V_p and $V_{\mu pore}$ results are observed after metal oxide extraction by DCB treatment. The volume-to-surface area ratios were used to calculate the average pore radius (R_p) for the general case of cylindrical pores ($R_p = 2\ V_p / SSA$) in Table 7. The interpretation of pore size in a slit configuration for calculating the radius ($R_p = V_p / SSA$) has been discussed with respect to continental shelf sediment (Mayer, 1994a). In Table 7, R_p values were determined in the mesopore range (2 nm to 50 nm) for WDC_{CB400} and $WDC_{DCB\ 400}$ samples were determined. The R_p of WDC_{CB400} decreased, indicating that the pore sizes were lower before than after metal oxide extraction. The coverage of metal oxide nanoparticles in accessible open mesopores, mainly formed by the arrangement of larger aluminosilicate particles such as the clay minerals illite or kaolinite in WDC (Table 1), can thus be concluded.

In Fig. 2, the cumulative pore volume and differential pore size distribution (PSD) curves with N_2 gas are reported in the case of Rollesbroich WDC_{CB70}, WDC_{CB400}, and $WDC_{DCB\ 400}$ samples which precisely determine the effects of metal oxide nanoparticles on the porosity in the low pore diameter range. A higher pore volume distribution in a pore diameter range < 25 nm was calculated for the WDC_{CB400} sample (25%) due to the presence of metal oxide nanoparticles in comparison with the WDC_{DCB400} sample (16%) in this soil. For the Selhausen and Wuestebach WDC samples, higher pore volume distributions in a pore diameter range < 25 nm of 35% and 25% were measured for WDC_{CB400} samples in comparison with 29% and 17%, respectively, for WDC_{DCB400} samples after metal oxide extraction which confirm that metal oxides will constrain the soil porous structure with lower pore size.

The detection of open pores by N_2 gas- adsorption was demonstrated when the presence of OC in pristine WDCs was considered. Significant differences in R_p were found between WDC_{CB70} and WDC_{CB400} which can be attributed to the presence of OC. The accessibility of N_2 gas to open pores is hindered by the blocking effect of OC (Mayer et al., 2004, McCarthy et al. 2008; Séquaris et al., 2010). This phenomenon can result in a shift in the distribution of open pores detected with N_2 gas to the greatest value in WDC_{CB70}, as shown by $R_{pCB70}/R_{pCB400} > 1$. In Fig. 2, for Rollesbroich soil, in pristine WDC_{CB70} sample, the

pore volume distribution in the pore diameter range > 25 nm is higher (80%) than in the WDC_{CB400} sample (75%). In the case of Selhausen and Wuestebach WDC samples, pore volume distributions in the pore diameter range > 25 nm of 70% and 76% are also found for WDC_{CB70} samples in comparison with 65% and 75%, respectively, for WDC_{CB400} samples after OC removal. These results support the preferential OC blocking effect in the low pore diameter range.

3.3.2. Effect of metal oxides on fractal dimensions of WDC measured with SAXS

The power-law behavior of the scattering SAXS resulted in a large range of ***q*:** $0.08nm^{-1}$ to 2 nm^{-1} (d =2*π/q of 3.1nm to78 nm) is observed in Fig. 3. The effect of metal oxides on the nature of the fractal structure of WDC was investigated with Eq. (7). The logarithmic form of the power-law scattering relation gives the exponent *k* (Fig. 3) by a least-squares fitting procedure.

In Table 8, *k* values ≤ 4 are calculated which indicates that conditions for a randomly oriented extended scatterer with uniform electron density and a smooth boundary surface (*k* = 4 for inhomogeneities with smooth separating surfaces) were not fulfilled with the WDC samples. *k* values between 3 and 4 characterize a rough interface of surface fractal dimensions D_s between 2 and 3 with Eq. (8). D_s values in the case of WDC_{DCB400} decrease significantly during DCB treatment, indicating that the surface roughness of the samples also decreases. Higher D_s values with WDC_{CB400} thus support the presence of nanoparticles causing the roughness of the pristine mineral surfaces or porosity with a low pore diameter range.

3.3.3. Contribution of metal oxide nanoparticles to the colloidal properties of mineral WDCs

The colloidal properties of WDC_{CB400} and WDC_{DCB400} were investigated after the dispersion of freeze-dried mineral WDC in water (0.4 g L^{-1}) by DLS and ME methods. The respective hydrodynamic diameter (d_z) and zeta potential (ζ) values at pH of about 7 ± 0.2 are reported in Table 8. In WDC_{DCB400} samples, the ζ values became more negative after the release of positively charged metal oxide particles. Metal oxide particles containing Fe and Al generally have points of zero charge of about pH 7 to 9 (Essington, 2004; Tombácz and Szekeres, 2001). The permanent negative charge of the remaining aluminosilicate, as in the case of illite clay minerals (Jiang et al., 2012), determines the ME properties of WDC_{DCB400}.The d_z values of WDC_{DCB400} samples increased compared with that of WDC_{CB400},

supporting the expansion of aggregate size due to electrostatic repulsion between negatively charged aluminosilicate residues. A possible aggregation of dispersed clay minerals through edge/plate (cardhouse structure) contacts (Lagaly et al., 2006; Jiang et al., 2012) under low ionic strength conditions may also increase d_z and the porosity. These colloidal results obtained on a micrometer scale can thus be directly related to k (SAXS), and R_p (N_2 gas-adsorption) results on a nanometer scale, also demonstrating a corresponding increase of the porous mineral matrix structure for the WDCs after the removal of metal oxide nanoparticles.

Systematically higher d_z, R_p and k values (Tables 7 and 8) are generally observed in the Rollesbroich WDC sample, which can be related to the mineralogical composition of the soil fraction < 2 μm in size. Indeed, higher kaolinite content than for the other two soil clay fractions (Table 1) was found in this soil. The contribution of the typically lower SSA of kaolinite than montmorillonite and illite (Manning and Goldberg, 1996) was also detected in the lowest SSA of the Rollesbroich WDC sample compared with the other soil samples (Table 6). In the Rollesbroich WDC sample, the introduction of the kaolinite particle structure of lower aspect ratios (Wilkinson and Lead, 2007) possibly creates large pores in the compact arrangement of dominant illite thin platelets of higher aspect ratios (ratio of platelet diameter to thickness) in the WDC microstructure. The calculated d_p (8 nm) of the metal oxide particles from the Rollesbroich WDCs sample (Table 3) was larger than that of the particles from Selhausen (5 nm) and Wuestebach (4 nm). This result supports a low steric hindrance for their formation and deposition in larger accessible WDC mesopores (R_p of 18 nm, Table 7).

4. Conclusion

The crystalline and less-crystalline iron oxides are the major metal oxide forms in the WDCs and bulk soils of the three topsoils investigated, and the highest distribution of less-crystalline iron oxide was observed in the acidic forest soil of Wuestebach. The decrease in SSA after the removal of metal oxides in the bulk soils and WDC samples is related to the released $M_{DCB\text{-}CB}$ and $M_{oxalate\text{-}blank}$ contents. Metal oxide nanoparticles (DCB extracted) of 4 nm to 8 nm in size (d_p) covered the surface of aluminosilicate residues in three soils and up to 22% of the WDCs from forest soil (Wuestebach). The results from the pore size (R_p) investigation of WDCs in freeze-dried state, using N_2 gas- adsorption, show that the presence of metal oxides in WDC_{CB400} implies the contraction of the pore structure in the low pore diameter range < 25 nm. Pore size distribution analysis also reveals a preferential blocking effect of the OC content in the same range of small open pore sizes. The characterization of

the fractal structure (from k exponent in Eq. (7)) of WDCs in freeze-dried state, using SAXS, indicates an increase of the surface fractal dimension (D_s) in the presence of metal oxides in $WDC_{CB400.}$ This result clearly supports an increase of the interface roughness in WDC due to the contributions of metal oxide nanoparticles.

The colloidal characterization of WDCs in a water-dispersed state from the three topsoils by DLS and ME methods also indicates that the measured colloidal particle size (d_z) and surface negative ζ-potential increased after the removal of metal oxides (DCB treatment). Results also indicate that the presence of positively charged metal oxides make the mineral matrix of WDC_{CB400} more compact, in the micrometer range, due to electrostatic interactions. Furthermore, the comparison of R_p, k, d_z and d_p results between soils also indicates some dependence of structure on the clay mineralogy of WDCs where effects of kaolinite and illite aspect ratios contribute to the mesopore size in the clay microfabric.

.The combination of the N_2 gas-adsorption, SAXS, DLS, and ME methods allows thus the porosity of air-dried and water-dispersed WDC to be characterized in the nanometer range where the large contribution of metal oxides can be detected and compared in different soils. The expansion of the SAXS method to include low scattering angles, the adsorption results of other gases as CO_2, and the use of improved models show great promise in enabling different pore structures and their distributions in soil aggregates to be described.

Acknowledgements

The presented work is part of the TERENO SoilCan project (Puetz et al., 2009). We would like to thank C. Walraf for her skilful laboratory assistance. The SAXS part of this work was supported by the Hungarian Scientific Research Fund (OTKA, Hungary) and the National Innovation Office (NIH, Hungary) under grant agreement CNK-81056, by the Hungarian Development Agency (NFÜ, Hungary) under grant agreement PT-0061 KMOP-1.1.2-07/1-2008-002, and by Gedeon Richter Plc, Hungary. We also wish to thank the University of Bonn (Dr. G. Welp, Institute of Soil Sciences, Agricultural Faculty) for the distribution analysis of particle sizes and the mineral XRD analysis. The elemental chemical analyses performed at the Central Division of Analytical Chemistry (ZCH) of Forschungszentrum Jülich Germany are gratefully acknowledged. Canlan Jiang thanks the Chinese Scholarship Council for the financial support of her PhD in Germany.

Reference

Baldock, J.A., Skjemstad, J.O., 2000. Role of the soil matrix and minerals in protecting natural organic materials against biological attack. Org. Geochem. 31, 697-710.

Bale, H.D., Schmidt, P.W., 1984. Small-Angle X-Ray-Scattering Investigation of Submicroscopic Porosity with Fractal Properties. Phys. Rev. Lett. 53(6), 596-599.

Barberis, E., Marsan, F.A., Boero, V., Arduino, E., 1991. Aggregation of soil particles by iron oxides in various size fractions of soil B horizons. J. Soil Sci.J. Soil Sci. 42(4), 535-542.

Blum, W.E.H., 2007. Bodenkunde in Stichworten. Gebr. Borntraeger Verlagsbuchhandlung, Berlin, Stuttgart, pp. 24-25.

Borggaard, O.K., 1982. The influence of iron oxides on the surface area of soil. J. Soil Sci. 33, 443-449.

Borkovec, M., Wu, Q., Degovics, G., Laggner, P., Sticher, H., 1993. Surface area and size distributions of soil particles. Colloids Surf., A 73, 65-76.

Campbell, A.S., Schwertmann, U., Stanjek, H., Friedl, J., Kyek, A., Campbell, P.A., 2002. Si incorporation into Hematite by heating Si-Ferrihydrite. Langmuir 18, 7804-7809

Chenu, C., Plante, A.F., 2006. Clay-size organo-mineral complexes in a cultivation chronosequence: revisiting the concept of the primary organo-mineral complex. Eur. J. Soil Sci. 57, 596-607.

Chevallier, T., Woignier, T., Toucet, J., Blanchart, E., 2010. Organic carbon stabilization in the fractal pore structure of Andosols. Geoderma 159(1–2), 182-188.

Childs, C.W., 1992. Ferrihydrite: A review of structure, properties and occurrence in relation to soils. Z.Pflanzenernaehr.Dueng.Bodenkd 155(5), 441-448.

Clausen, L., Fabricius, I., 2000. BET measurements: outgassing of minerals.J. Colloid Interface Sci. 227(1), 7-15.

Cornell, R.M., Schwertmann, U., 1996. The iron oxides-structure, properties, reactions, occurrence and uses. VCH, New York.

Cornell, R.M., Schwertmann, U., 2003. The Iron Oxides: Structure, Properties. Reactions, Occurrence and Uses, 2nd Edition. Wiley-VCH Verlag GmbH & Co. KGaA, Weinheim.

Deshpande, T.L., Greenland, D.J., Quirk, J.P., 1968. Charges in soil properties associated with the removal of iron and aluminium oxides J. Soil Sci. 19, 108-122.

Dékány, I., Turi, L., Fonseca, A., Nagy, J.B., 1999. The structure of acid treated sepiolites: small-angle X-ray scattering and multi MAS-NMR investigations. Appl.Clay Sci. 14(1–3), 141-160.

Driessen, P., Deckers, J., Spaargaren, O., Nachtergaele, F., 2001. Lecture notes on the major soils of the world. World Soil Resources Reports.

Essington, M. E. (2004). Soil and water chemistry: An integrative approach. CRC press. Boca Raton, Florida, pp. 328.

Eusterhues, K., Rumpel, C., Kögel-Knabner, I., 2005. Organo-mineral associations in sandy acid forest soils: importance of specific surface area, iron oxides and micropores. Eur. J. Soil Sci. 56(6), 753-763.

Filimonova, S.V., Knicker, H., Kögel-Knabner, I., 2006. Soil micro- and mesopores studied by N_2 adsorption and ^{129}Xe NMR of adsorbed xenon. Geoderma 130(3-4), 218-228.

Gaboriaud, F., Ehrhardt, J.-J., 2003. Effects of different crystal faces on the surface charge of colloidal goethite (α-FeOOH) particles: an experimental and modeling study. Geochim. Cosmochim. Acta 67(5), 967-983.

Gilkes, R., Scholz, G., Dimmock, G., 2006. Lateritic deep weathering of granite. J. Soil Sci. 24(4), 523-536.

Goldberg, S., 1989. Interaction of aluminum and iron oxides and clay minerals and their effect on soil physical properties: A review. Commun. Soil Sci. Plant Anal. 20(11-12), 1181-1207.

Groen, J.C., Peffer, L.A.A., Pérez-Ramírez, J., 2003. Pore size determination in modified micro-andmesoporous materials. Pitfalls and limitations in gas adsorption data analysis. Microporous Mesoporous Mater. 60(1), 1-17.

Guinier, A., Fournet, G., 1955. Small Angle Scattering of X-rays. J. Wiley & Sons, New York.

Hendershot, W.H., Lavkulich, L.M., 1983. Effect of sesquioxide coatings on surface charge of standard mineral and soil samples. Soil Sci. Soc. Am. J. 47, 1252-1260.

Herbst, M., Welp, G., Vereecken, H., & Amelung, W. (2011). Rock fragments control size and saturation of organic carbon pools in agricultural topsoil. Soil Sci. Soc. Am. J. 75(5), 1898-1907.

Hiemstra, T., Antelo, J., Rahnemaie, R., Riemsdijk, W.H.v., 2010a. Nanoparticles in natural systems I: The effective reactive surface area of the natural oxide fraction in field samples. Geochim. Cosmochim. Acta 74(1), 41-58.

Höhr, A., Neumann, H.-B., Schmidt, P.W., Pfeifer, P., Avnir, D., 1988. Fractal surface and cluster structure of controlled-pore glasses and Vycor porous glass as revealed by small-angle x-ray and neutron scattering. Physical Review B 38(2), 1462-1467.

IUPAC, 1985, Reporting physisorption data for gas/solid systems with special reference for the determination of surface area and porosity. Pure Appl. Chem. 57(4), 603-619.

Jarvis, N.J., Villholth, K.G., Ulén, B., 1999. Modelling particle mobilization and leaching in macroporous soil. Eur. J. Soil Sci. 50, 621-632.

Jiang, C., Séquaris, J.-M., Vereecken, H., Klumpp, E., 2012. Effects of inorganic and organic anions on the stability of illite and quartz soil colloids in Na-, Ca- and mixed Na-Ca systems. Colloids Surf., A 415, 134-141.

Jiang, C., Séquaris, J. -M., Vereecken, H., Klumpp, E., 2013. Diffusion-controlled mobilization of water-dispersible colloids from three German silt loam topsoils: effect of temperature, Eur. J. Soil Sci. 64(6), 777-786.

Kaiser, K., Guggenberger, G., 2000. The role of DOM sorption to mineral surfaces in the preservation of organic matter in soils. Org. Geochem. 31(7-8), 711-725.

Kaiser, K., Guggenberger, G., 2003. Mineral surfaces and soil organic matter. Eur. J. Soil Sci. 54(2), 219-236.

Kiem, R., Knicker, H., Kögel-Knabner, I., 2002. Refractory organic carbon in particle-size fractions of arable soils I: distribution of refractory carbon between the size fractions. Org. Geochem. 33(12), 1683-1697.

Kiem, R., Kögel-Knabner, I., 2002. Refractory organic carbon in particle-size fractions of arable soils II: organic carbon in relation to mineral surface area and iron oxides in fractions < 6 µm. Org. Geochem. 33(12), 1699-1713.

Kjaergaard, C., de Jonge, L.W. Moldrup, P., Schjonning, P., 2004a. Water-dispersible colloids: effects of measurement method, clay content, initial soil matric potential, and wetting rate. Vadose Zone J. 3, 403-412.

Kjaergaard, C., Hansen, H.C.B., Koch C.B., Villholth, K.G., 2004b. Properties of water-dispersible colloids from macropore deposits and bulk horizons of an agrudalf. Soil Sci. Soc. Am. J. 68, 1844-1852.

Kleber, M., Mikutta, R., Torn, M.S., Jahn, R., 2005. Poorly crystalline mineral phases protect organic matter in acid subsoil horizons. Eur. J. Soil Sci. 56(6), 717-725.

Kretzschmar, R., Robarge, W.P., Weed, S.B., 1993. Flocculation of kaolinitic soil clays: effects of humic substances and iron oxides. Soil Sci. Soc. Am. J. 57(5), 1277-1283.

R. Kretzschmar, M. Borkovec, D. Grolimund, M. Elimelech, 1999 Mobile subsurface colloids and their role in contaminant transport, in Advances in Agronomy, Vol 66. Academic Press, San Diego. pp. 121-193.

Lagaly, G. Colloid clay science, in: F. Bergaya, B.K.G. Theng, G. Lagaly (Eds.), Handbook of Clay Science, Elsevier, Amsterdam, 2006, pp. 141-245.

Lowell, S., Shields, J., Thomas, M., Thommes, M., 2006. Characterization of Porous Solids and Powders: Surface Area, Pore Size and Density. Particle Technology Series. Springer Netherlands.

Manning, B.A., Goldberg, S., 1996. Modeling arsenate competitive adsorption on kaolinite, montmorillonite and illite. Clays Clay Miner. 44(5), 609-623.

Marliere, C., Woignier, T., Dieudonné, P., Primera, J., Lamy, M., Phalippou, J., 2001. Two fractal structures in aerogel. Journal of non-crystalline solids, 285(1), 175-180.
Masiello, C.A., Chadwick, O.A., Southon, J., Torn, M.S., Harden, J.W., 2004. Weathering controls on mechanisms of carbon storage in grassland soils. Global Biogeochem. Cycles 18(4), GB4023.
Mayer, L.M., 1994a. Surface area control of organic carbon accumulation in continental shelf sediments. Geochim. Cosmochim. Acta. 58, 1271-1284.
Mayer, L.M., 1994b. Relationships between mineral surfaces and organic carbon concentrations in soils and sediments. Chemical Geology. 114(3-4), 347-363.
Mayer, L.M., Schick, L.L., Hardy, K.R., Wagai, R., McCarthy, J., 2004. Organic matter in small mesopores in sediments and soils. Geochim. Cosmochim. Acta 68(19), 3863-3872.
J.F. McCarthy, J.M. Zachara, 1989, Subsurface transport of contaminants. Environ. Sci. Technol., 23(5), 496-502.
McCarthy, J.F., Ilavsky, J., Jastrow, J.D., Mayer, L.M., Perfect, E., Zhuang, J., 2008. Protection of organic carbon in soil microaggregates via restructuring of aggregate porosity and filling of pore with accumulating organic matter. Geochim. Cosmochim. Acta 72, 4725-4744.
Mehra, O.P., Jackson, M.L., 1960. Iron oxide removal from soils and clays by dithionite-citrate system bufferd with sodium bicarbonate, Clays Clay Miner. Proceedings of the 7th National Conference, pp. 317-327.
Mikutta, R., Kleber, M., Jahn, R., 2005. Poorly crystalline minerals protect organic carbon in clay subfractions from acid subsoil horizons. Geoderma 128(1-2), 106-115.
Mikutta, R., Kleber, M., Torn, M.S., Jahn, R., 2006. Stabilization of soil organic matter: association with minerals or chemical recalcitrance? Biogeochemistry 77(1), 25-56.
Mikutta R, Mikutta C, Kalbitz K, Scheel T, Kaiser K, Jahn R 2007 Biodegradation of forest floor organic matter bound to minerals via different binding mechanisms. Geochim. Cosmochim. Acta 71, 2569-2590.
Mittelbach, P., 1964. Zur Röntgenkleinwinkelstreuung verdünnter kolloider systeme:VIII Diskussion des Streuverhaltens regelmäÿiger Körper und Methoden zur Bestimmung von Gröÿe und Form kolloider Teilchen. Acta Phys. Anstriaca 19, 53-102.
Pernyeszi, T., Dékány, I., 2003. Surface fractal and structural properties of layered clay minerals monitored by small-angle X-ray scattering and low-temperature nitrogen adsorption experiments. Colloid. Polym. Sci. 281(1), 73-78.
Pinheiro-Dick, D., Schwertmann, U., 1996. Microaggregates from Oxisols and Inceptisols: dispersion through selective dissolutions and physicochemical treatments. Geoderma 74(1-2), 49-63.
Pronk, G.J., Heister, K., Kögel-Knabner, I., 2011. Iron Oxides as Major Available Interface Component in Loamy Arable Topsoils. Soil Sci. Soc. Am. J. 75(6), 2158-2168.
Puetz, T., Burauel, P., Bogena, H., Vereecken, H., 2009. TERENO-SoilCan-Soil-Atmosphere Interactions Induced by Land Use Changes as a Result of Global Change, EGU General Assembly Conference Abstracts, pp. 11611.
Radlinski, A.P., Mastalerz, M., Hinde, A.L., Hainbuchner, M., Rauch, H., Baron, M., Lin, J.S., Fan, L., Thiyagarajan, P., 2004. Application of SAXS and SANS in evaluation of porosity, pore size distribution and surface area of coal. Int. J. Coal Geol. 59(3-4), 245-271.
Roden, E.E., Zachara, J.M., 1996. Microbial reduction of crystalline iron (III) oxides: Influence of oxide surface area and potential for cell growth. Environ. Sci. Technol. 30(5), 1618-1628.
Rosenqvist, J., Axe, K., Sjöberg, S., Persson, P., 2003. Adsorption of dicarboxylates on nano-sized gibbsite particles: effects of ligand structure on bonding mechanisms. Colloids Surf., A 220(1–3), 91-104.
Ryan, J.N., Gschwend, P.M., 1994. Effects of ionic strength and flow rate on colloid release: relating kinetics to intersurface potential energy. J. Colloid Interface Sci. 164, 21-34.
Ryan, J.N., Elimelech, M., 1996. Colloid mobilization and transport in groundwater. Colloids Surf., A, 107, 1-56.
Saunders, J.M., Goodwin, J.W., Richardson, R.M., Vincent, B., 1999. A Small-Angle X-ray Scattering Study of the Structure of Aqueous Laponite Dispersions. J.Phys.Chem.B 103(43), 9211-9218.

Schahabi, S., Schwertmann, U., 1970. Der Einfluß von synthetischen Eisenoxiden auf die Aggregation zweier Lößbodenhorizonte. Z.Pflanzenernaehr.Dueng.Bodenkd 125(3), 193-204.

Schmidt, P., 1991. Small-angle scattering studies of disordered, porous and fractal systems. J. Appl. Crystallogr. 24(5), 414-435.

Schmidt, P.W., Avnir, D., Levy, D., Höhr, A., Steiner, M., Röll, A., 1991. Small-angle x-ray scattering from the surfaces of reversed-phase silicas: Power-law scattering exponents of magnitudes greater than four. J. Chem. Phys. 94, 1474.

Schwertmann, v.U., 1964. The differentiation of iron oxide in soils by a photochemical extraction with acid ammonium oxalate. Z. Pflanzenernaehr. Dueng. Bodenkd 105, 194-201.

Séquaris, J.-M., Guisado, G., Magarinos, M., Moreno, C., Burauel, P., Narres, H.-D., Vereecken, H., 2010. Organic-carbon fractions in an agricultural topsoil assessed by the determination of the soil mineral surface area. J. Plant Nutr. Soil Sci. 173(5), 699-705.

Séquaris, J.-M., Klumpp, E., Vereecken, H., 2013. Colloidal properties and potential release of water-dispersible colloids in an agricultural soil depth profile. Geoderma 193, 94-101.

Séquaris, J.M., Lewandowski, H., 2003. Physicochemical characterization of potential colloids from agricultural topsoils. Colloids Surf., A 217(1-3), 93-99.

Six, J., Conant, R.T., Paul, E.A., Paustian, K., 2002. Stabilization mechanisms of soil organic matter: Implications for C-saturation of soils. Plant Soil 241, 155-176.

Sollins, P., Homann, B., Caldwell, A., 1996. Stabilization and destabilization of soil organic matter: mechanisms and controls. Geoderma 74, 65-105.

Sollins, P., Swanston, C., Kramer, M., 2007. Stabilization and destabilization of soil organic matter—a new focus. Biogeochemistry 85(1), 1-7.

Tombácz, E., Szekeres, M., 2001. Interfacial Acid−Base Reactions of Aluminum Oxide Dispersed in Aqueous Electrolyte Solutions. 1. Potentiometric Study on the Effect of Impurity and Dissolution of Solid Phase. Langmuir 17(5), 1411-1419.

Trolard, F., Bourrie, G., Jeanroy, E., Herbillon, A.J., Martin, H., 1995. Trace metals in natural iron oxides from laterites: A study using selective kinetic extraction. Geochim. Cosmochim. Acta 59(7), 1285-1297.

Turchenek, L. W., Oades, J. M., 1979. Fractionation of organo-mineral complexes by sedimentation and density techniques. Geoderma 21(4), 311-343.

Wagai, R., Mayer, L.M., 2007. Sorptive stabilization of organic matter in soils by hydrous iron oxides. Geochim. Cosmochim. Acta 71(1), 25-35.

Wagai, R., Mayer, L. M., & Kitayama, K., 2009. Extent and nature of organic coverage of soil mineral surfaces assessed by a gas sorption approach.Geoderma 149(1), 152-160.

Wilkinson, K.J., Lead, J.R., 2007. Environmental colloids and particles: behaviour, separation and characterisation, 10. Wiley, USA.

Zacharias, S., Bogena, H., Samaniego, L., Mauder, M., Fuß, R., Pütz, T., Frenzel, M., Schwank, M., Baessler, C., Butterbach-Bahl, K., 2011. A network of terrestrial environmental observatories in Germany. Vadose Zone J. 10(3), 955-973.

Van Oost, K., Govers, G., Quine, T.A., Heckrath, G., Olesen, J.E., De Gryze, S., et al. 2005. Landscape-scale modeling of carbon cycling under the impact of soil redistribution: the role of tillage erosion. Glob. Biogeochem. Cycles 19c, GB4014.

Fig. 1. A schematic diagram of the soil samples preparation

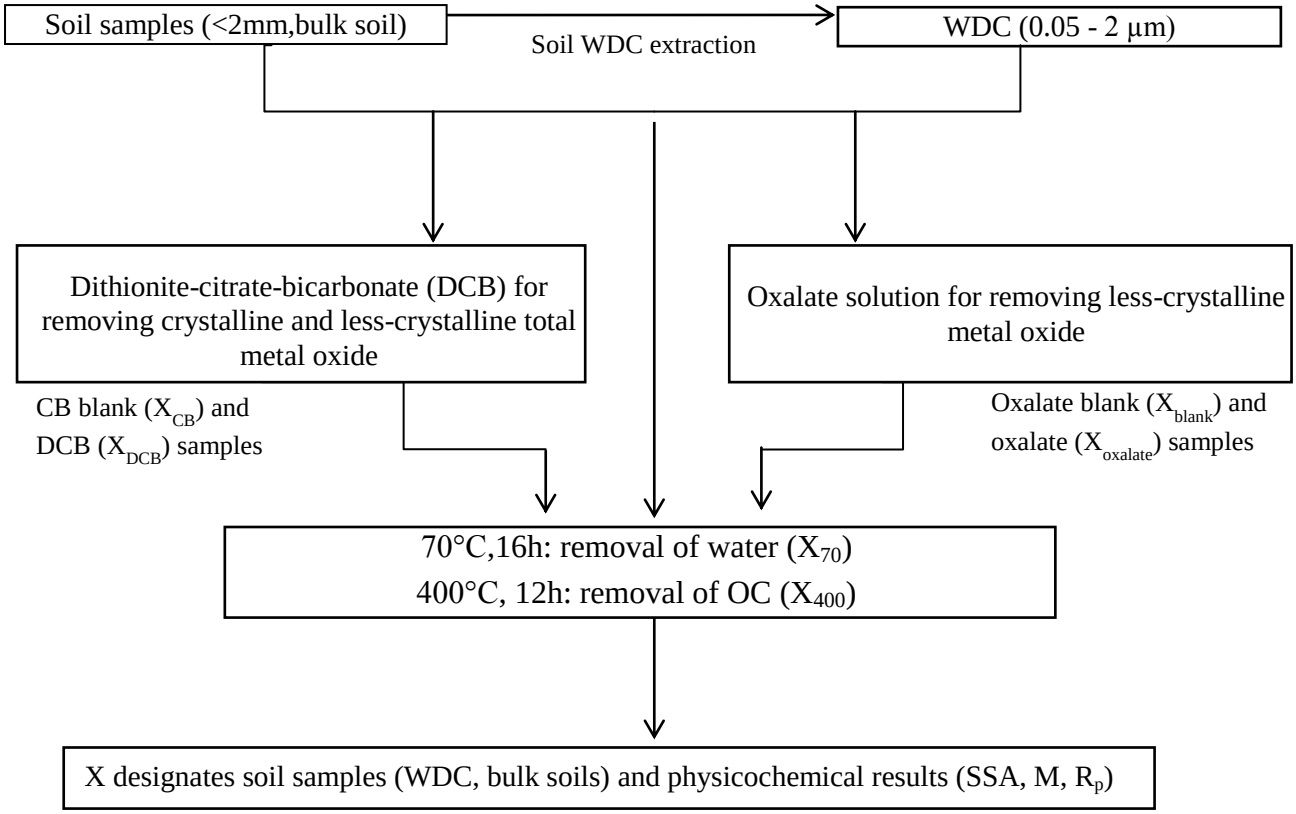

Fig. 1.

Fig. 2. Cumulative pore volume and differential pore-size distribution (PSD) curves of WDC samples from Rollesbroich topsoil measured with N_2 gas sorption (BJH method).. ——, WDC_{CB400} ; -----, WDC_{DCB400} ; **……**, WDC_{CB70} (see also text).

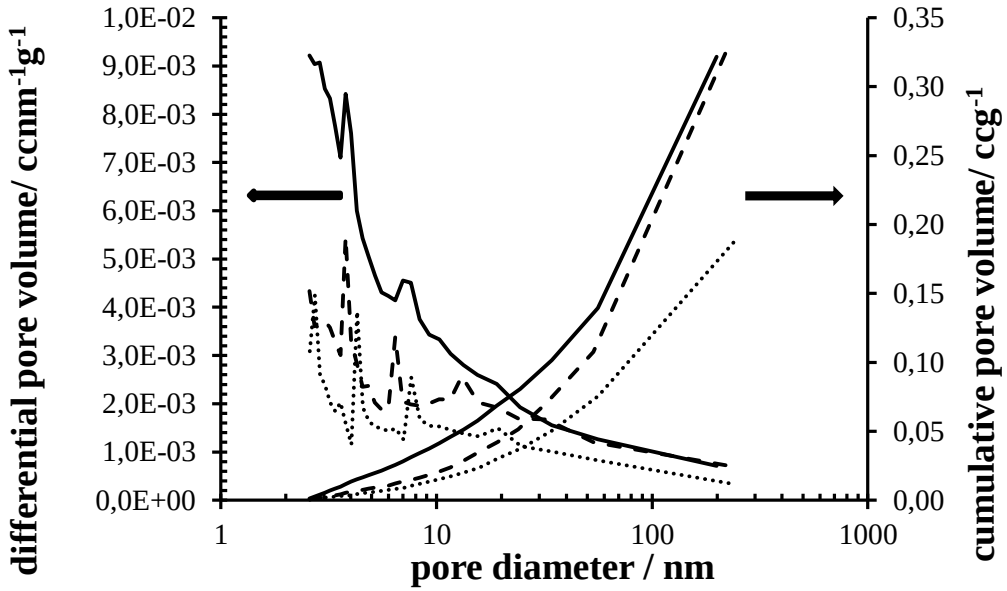

Fig. 2.

Fig. 3. SAXS scattering curves (log $I(q)$ vs log q) of WDCs from Wuestebach topsoil after CB and DCB treatments being followed by the thermal oxidation of organic matter. ·····, WDC_{DCB400}; -----, WDC_{CB400}. Linear least-squares fitting of Eq. (8) in the range of $q < 2$ nm^{-1} was applied.

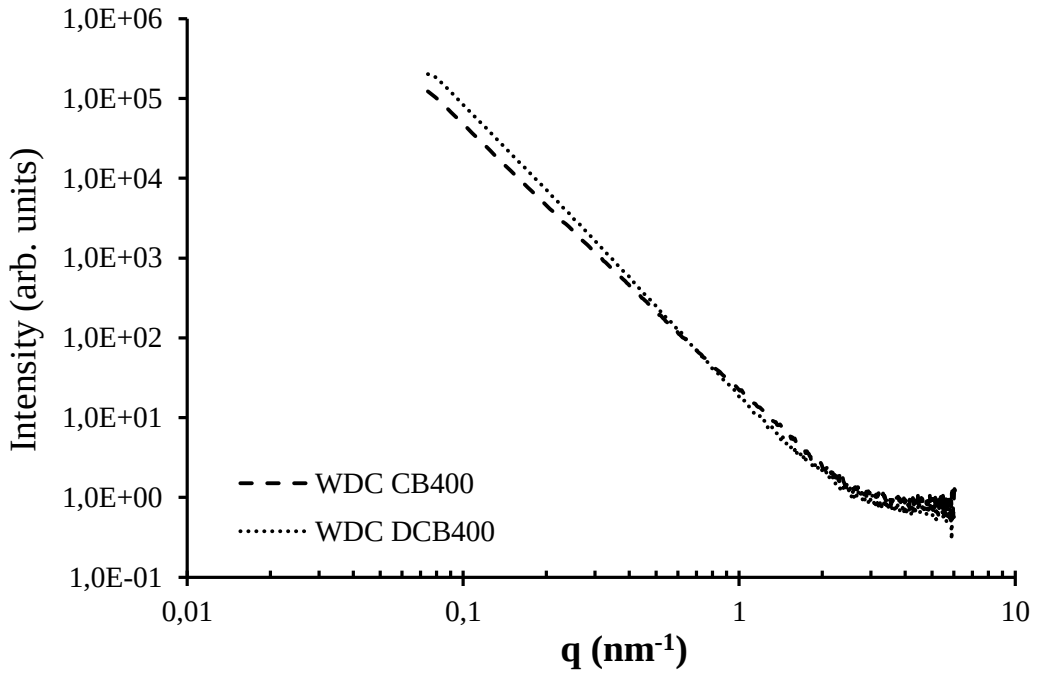

Fig. 3.

Table 1 Soils physicochemical characteristics.

Soil	pH [a]	TOC [b] g kg^{-1}	TN g kg^{-1}	Fe g kg^{-1}	Al g kg^{-1}	Si g kg^{-1}	Clay %	Silt %	Sand %	Minerals in clay fraction[c]
Selh	7.07	10.0 ± 0.2	1.07 ± 0.05	25.7	44.4	355	19	65.6	15.7	I^{A}, C/V^{B}, K^{C}
Roll	5.82	40.4 ± 1.7	4.62 ± 0.09	26.2	58.0	324	20	59.2	20.8	I^{A}, K^{B}, C/V^{C}
Wuest	4.25	83.1 ± 2.5	6.10 ± 0.40	35.9	65.5	266	21	60.2	18.5	I^{A}, C/V^{B}, K^{C}

[a] soil / water = 1 / 2.5; [b] values are average of three different experiments ± standard deviation; [c] XRD mineral analysis: I, illite; C/V, chlorite and/ or vermiculite; K, kaolinite; ^{A} = abundant; ^{B} = present; ^{C} = little

Table 2 Comparison of specific surface area (SSA) of Selhausen bulk soils after temperature pre-treatment.

Soil samples	Clay / %	*TOC* / g kg^{-1}	Fe_{DCB} / g kg^{-1}	SSA_{70} / m^2 g^{-1}	SSA_{400} / m^2 g^{-1}	SSA_{70} / SSA_{400}
C1 (0-30 cm)	18.3	11.3 ± 0.6	7.7 ± 0.4	12.8	15.2	0.84
C1(30-60 cm)	21.7	3.6 ± 0.2	9.2 ± 0.2	23.2	22.3	1.04
C1(60-90 cm)	21.7	2.3 ± 0.2	10.3 ± 0.3	22.8	21.7	1.05
C2 (0-30 cm)	12.3	12.6 ± 0.3	6.9 ± 0.3	7.8	8.1	0.96
C2(30-60 cm)	15.7	5.6 ± 0.1	6.8 ± 0.3	9.7	11.9	0.82
C2(60-90 cm)	17	4.2 ± 0.4	7.5 ± 0.5	10.8	9.7	1.11

Table 3:Physicochemical characteristics for WDC and metal oxide content

		WDC					metal oxide content			
	pH	mass in bulk soil [a]	TOC [a]	Fe	Al	Si	w^b	$SSA_{metal\ oxide}$	Θ^c	d_p [d]
		g kg^{-1}	g kg^{-1}	g kg^{-1}	g kg^{-1}	g kg^{-1}	g kg^{-1}	m^2 g^{-1}	%	nm
Selh	7.4	81±2	21.7±0.1	75	115	207	84±9	342	11.1	5
Roll	6.6	41±2	67.74±1.1	55.6	124	163	93±5	217	15.6	8
Wuest	4.5	41±1	71.25±0.1	75. 9	124	173	76±16	420	21.6	4

[a] values are average of three different experiments ± standard deviation .[b]mass of released metal oxide from WDC. [c]surface loading ratio of metal oxide Eq. (4). [d]diameter of metal oxide particle Eq. (6)

Table 4 CB and DCB extracted metals contents in WDC and bulk soil samples.

Soil	Fraction	M_{CB} mg g^{-1} [a]			M_{DCB} mg g^{-1} [a]			M_{DCB-CB} mg g^{-1} [a]		
		Al	Fe	Si	Al	Fe	Si	Al	Fe	Si
Selh	Bulk soil	0.18±0.04	0.31±0.01	0.23±0.12	1.07±0.04	11.75±0.48	0.56±0.01	0.89±0.05	11.44±0.48	0.33±0.12
	WDC	0.57±0.02	0.91±0.06	0.39±0.04	3.93±0.05	39.47±0.71	1.64±0.03	3.36±0.06	38.56±0.72	1.26±0.05
Roll	Bulk soil	1.63±0.01	2.35±0.03	0.20±0.01	3.31±0.10	16.68±0.64	0.33±0.04	1.68±0.10	14.33±0.64	0.13±0.04
	WDC	6.68±0.18	14.7±0.29	0.52±0.01	11.73±3.38	56.54±15.10	0.75±0.15	5.04±3.38	41.80±15.1	0.23±0.15
Wuest	Bulk soil	3.85±0.01	7.49±0.16	0.91±0.01	5.71±0.22	26.26±1.66	0.79±0.02	1.87±0.21	18.77±1.67	0.1±0.02
	WDC	4.45±0.12	5.24±0.12	0.36±0.07	9.37±1.87	45.12±8.55	0.67±0.14	4.91±1.87	39.89±8.55	0.31±0.16

[a] values are average of three different experiments ± standard deviation.

Table 5 Oxalate extracted metal contents in WDC and bulk soil samples and their distribution in total metal oxides.

Soil	Fraction	M_{blank} mg g^{-1}			$M_{oxalate}$mg g^{-1} [a]			$M_{oxalate}/M_{DCB}$
		Al	Fe	Si	Al	Fe	Si	Fe
Selh	Bulk soil	0.04	0.03	0.12	0.88±0.03	3.36±0.19	0.21±0.01	0.29
	WDC	0.03	0.02	0.14	3.74±0.01	11.5±0.05	0.85±0.01	0.29
Roll	Bulk soil	0.03	0.01	0.04	2.60±0.02	6.43±0.17	0.11±0.01	0.38
	WDC	0.02	0.03	0.07	8.11±0.05	14.6±0.12	0.33±0.01	0.26
Wuest	Bulk soil	0.08	0.05	0.04	4.17±0.28	11.9±0.84	0.11±0.01	0.45
	WDC	0.22	0.17	0.26	8.77±0.14	24.3±0.58	0.36±0.01	0.54

[a] values are average of three different experiments ± standard deviation.

Table 6 The measured specific surface areasusing N_2 gas- adsorption method forWDC and bulk soil samples from three topoils.

Soils		Metal oxide$_{DCB}$			Metal oxide$_{oxalate}$		
		SSA_{CB70}/ SSA_{CB400}	SSA_{DCB70}/ SSA_{DCB400}	$SSA_{((CB-DCB)/CB)400}$	$SSA_{blank70}$/ $SSA_{blank400}$	$SSA_{oxalate70}$/ $SSA_{oxalate400}$	$SSA_{((blank-oxalate)/blank)400}$
		$m^2\ g^{-1}$	$m^2\ g^{-1}$	%	$m^2\ g^{-1}$	$m^2\ g^{-1}$	%
Selh	Bulk soil	5.3/ 10.4	4.9/ 6.2	41	12.8/ 18.8	6.1/ 15.8	16
	WDC	58.1/ 87.7	34.5/ 64.3	27	66.7/ 87.4	37.3/ 83.2	5
Roll	Bulk soil	7.0/ 15.8	4.9/ 9.0	43	7.6/ 23.1	5.6/ 15.2	34
	WDC	25.1/ 49.2	20.2/ 32.1	35	30.9/ 69.7	21.8/ 59.8	14
Wuest	Bulk soil	8.3/ 17.1	5.3/ 9.5	45	14.1/ 29.6	5.8/ 19.3	35
	WDC	36.6/ 66.5	20.6/ 37.2	44	55.5/ 87.3	23.2/ 67.8	22

Table 7 Pore size investigation of WDCs using N_2 gas- adsorption methodforWDC_{CB70}， WDC_{CB400}， and WDC_{DCB400} samples from three topoils.

	Sample	*SSA* m^2g^{-1}	$V_{\mu pore}$ $cm^3\ g^{-1}$	Total V_{pore} cm^3g^{-1}	$R_{p(N_2)}$ nm	$R_{p\mathrm{DCB400}}/R_{p\mathrm{CB400}}$	$R_{p\mathrm{CB70}}/R_{p\mathrm{CB400}}$	PSD Pore < 25nm (%)	PSD Pore >25nm (%)
Selh	WDC_{CB70}	58.1	0.014	0.23	9.53	1.17	1.36	30	70
	WDC_{CB400}	87.7	0.025	0.31	7.02			35	65
	WDC_{DCB400}	64.3	0.020	0.27	8.23			29	71
Roll	WDC_{CB70}	25.1	0.007	0.19	17.43	1.40	1.38	20	80
	WDC_{CB400}	49.2	0.015	0.33	12.62			25	75
	WDC_{DCB400}	32.1	0.009	0.37	17.68			16	84
Wuest	WDC_{CB70}	36.6	0.008	0.21	13.51	1.46	1.28	24	76
	WDC_{CB400}	66.5	0.020	0.31	10.56			25	75
	WDC_{DCB400}	37.2	0.009	0.27	15.38			17	83

Table 8 Pore structure characteristics (k, D_S) and colloidal properties (d_z , ζ-potential) of WDC samples measured with SAXS, DLS and ME methods.

Sample name	SAXS			DLS and ME		
	power-law scattering			pH	d_z(nm)[c]	ζ (mV)[c]
	k[a]	D_s[b]	r^2			
Selh WDC_{CB400}	3.31±0.01	2.69±0.01	1	7.13	542±11	-28.9±0.4
Selh WDC_{DCB400}	3.60±0.01	2.40±0.01	1	6.91	639±1	-29.6±0.4
Roll WDC_{CB400}	3.48±0.01	2.52±0.01	1	7.10	721±30	-26.9±0.7
Roll WDC_{DCB400}	3.80±0.01	2.20±0.01	1	6.89	769±19	-28.1±0.1
Wüst WDC_{CB400}	3.30±0.01	2.70±0.01	1	7.26	715±28	-26.9±0.0
Wüst WDC_{DCB400}	3.70±0.01	2.30±0.01	1	7.17	802±11	-32.5±0.8

[a]linear fitting results of Eq. (7).
[b] D_s results with Eq. (8).
[b] values are average of three different experiments ± standard deviation.